

Which spectral distortions does Λ CDM actually predict?

Jens Chluba¹*

¹ Jodrell Bank Centre for Astrophysics, University of Manchester, Oxford Road, Manchester M13 9PL, UK

Accepted 2016 April 18. Received 2016 March 12

ABSTRACT

Ever refined cosmological measurements have established the Λ CDM concordance model, with the key cosmological parameters being determined to percent-level precision today. This allows us to make explicit *predictions* for the spectral distortions of the cosmic microwave background (CMB) created by various processes occurring in the early Universe. Here, we summarize all *guaranteed* CMB distortions and assess their total uncertainty within Λ CDM. We also compare simple methods for approximating them, highlighting some of the subtle aspects when it comes to interpreting future distortion measurements. Under simplified assumptions, we briefly study how well a *PIXIE*-like experiment may measure the main distortion parameters (i.e., μ and y). Next generation CMB spectrometers are expected to detect the distortion caused by reionization and structure formation at extremely high significance. They will also be able to constrain the small-scale power spectrum through the associated μ -distortion, improving limits on running of the spectral index. Distortions from the recombination era, adiabatic cooling of matter relative to the CMB and dark matter annihilation require a higher sensitivity than *PIXIE* in its current design. The crucial next step is an improved modeling of foregrounds and instrumental aspects, as we briefly discuss here.

Key words: Cosmology: cosmic microwave background – theory – observations

1 INTRODUCTION

The standard Λ CDM cosmology has been shown to describe our Universe to extremely high accuracy (Bennett et al. 2003; Planck Collaboration et al. 2014d, 2015b). This model is based upon a spatially flat, expanding Universe with dynamics governed by General Relativity and whose dominant constituents at late times are cold dark matter (CDM) and a cosmological constant (Λ). The primordial seeds of structures are furthermore Gaussian-distributed adiabatic fluctuations with an almost scale-invariant power spectrum thought to be created by inflation.

Today, we know the key cosmological parameters (e.g., the total, CDM and baryon densities, the CMB photon temperature, Hubble expansion rate, etc.) to percent-level precision or better (Planck Collaboration et al. 2015b). Assuming standard Big Bang Nucleosynthesis (BBN) and a standard thermal history, we can furthermore derive precise values for the helium abundance, Y_p , and effective number of relativistic degrees of freedom, N_{eff} (e.g., Steigman 2007). Also the physics of the recombination era, which defines the decoupling of photons and baryons around redshift $z \approx 10^3$, is now believed to be well understood within Λ CDM (e.g., Chluba & Thomas 2011; Ali-Haïmoud & Hirata 2011).

Of the many cosmological data sets, measurements of the cosmic microwave background (CMB) temperature and polarization anisotropies, beyond doubt, have driven the development towards precision cosmology over the few past years. Today, cos-

mologists have exhausted practically all information about the primordial Universe contained in the CMB temperature power spectra. *WMAP* and *Planck* have also clearly seen the *E*-mode polarization signals (Page et al. 2007; Planck Collaboration et al. 2014c, 2015c). Several sub-orbital and space-based experiments (e.g., *BICEP3*, *CLASS*, *SPTpol*, *ACTpol*, *SPIDER*, *PIPER*, *LiteBird*, *PIXIE*, *COrE+*) are now rushing to detect the primordial *B*-modes at large angular scales and to squeeze every last bit of information out of the *E*-mode signals, all to deliver the long-sought proof of inflation.

It is well known that CMB *spectral distortions* – tiny departures of the average CMB energy spectrum from that of a perfect blackbody – deliver a new independent probe of different processes occurring in the early Universe. The case for spectral distortions has been made several times and the physics of their formation is well understood (for recent overview see, Chluba & Sunyaev 2012; Sunyaev & Khatri 2013; Chluba 2013a; Tashiro 2014; De Zotti et al. 2015). The purpose of this article is to provide an overview of all distortion signals created within Λ CDM (Fig. 1), also assessing their total uncertainty. Although non-standard processes (i.e., decaying particles or evaporating primordial black holes) could cause additional interesting signals, the Λ CDM distortions define clear targets for designing future distortion experiments.

Thus far, no all-sky distortion has been found (Fixsen et al. 1996; Fixsen 2009), however, new experimental concepts, such as *PIXIE* (Kogut et al. 2011), are being actively discussed and promise improvements of the measurements carried out with *COBE/FIRAS* by several orders of magnitude. It is thus time to ask what new information could be extracted from the CMB spectrum and how this could help refine our understanding of the Universe.

* E-mail: Jens.Chluba@manchester.ac.uk

The case for spectral distortions as a new independent probe of inflation has also been made several times (e.g., Hu & Silk 1993a; Chluba et al. 2012b,a; Dent et al. 2012; Pajer & Zaldarriaga 2013; Khatri & Sunyaev 2013; Chluba & Grin 2013; Chluba 2013a; Clesse et al. 2014), most recently by Cabass et al. (2016), who emphasized that, given the constraints from *Planck*, an improvement in the sensitivity by a factor of ≈ 3 over *PIXIE* guarantees either a detection of μ or of negative running ($\gtrsim 95\%$ c.l.). Here we add a few aspects to the discussion related to the interpretation of future distortion measurements carried out with an instrument similar to *PIXIE*. For real distortion parameter estimation, one has to simultaneously determine the average CMB temperature, μ , y and residual (r -type) distortion parameters, as well as several foreground parameters from measurements in different spectral bands (Chluba & Jeong 2014). In this case, estimates for μ and y based on simple scattering physics arguments (Sect. 3.1) underestimate the experimentally recovered (\leftrightarrow measured) parameters, as we illustrate here.

We also briefly illustrate how well a *PIXIE*-like experiment may be able to constrain power spectrum parameters through the associated μ -distortion when combined with existing constraints from *Planck* (Planck Collaboration et al. 2015b). We find that an experiment with ≈ 3.4 times the sensitivity of *PIXIE* in its current design (Kogut et al. 2011) could allow tightening the constraint on the running of the spectral index by $\approx 40\% - 50\%$ when combined with existing data. This would also deliver an $\approx 5\sigma$ detection of the μ -distortion from CMB distortions alone. An ≈ 10 times enhanced sensitivity over *PIXIE* would furthermore allow a marginal detection of the first residual distortion parameter, which could be crucial when it comes to distinguishing different sources of distortions.

These forecasts are very idealized, assuming that the effective channel sensitivity already includes the penalty paid for foreground separation. Clearly, a more detailed foreground modeling for the monopole is required to demonstrate the full potential of future spectroscopic CMB missions, as we briefly discuss in Sect. 4.1. However, we argue that a combination of different data sets and exploitation of the many spectral channels of *PIXIE* will hopefully put us into the position to tackle this big challenge in the future.

2 SPECTRAL DISTORTIONS WITHIN Λ CDM

Several exhaustive overviews on various spectral distortion scenarios exist (Chluba & Sunyaev 2012; Sunyaev & Khatri 2013; Chluba 2013a; Tashiro 2014; De Zotti et al. 2015), covering both standard and non-standard processes. Here we only focus on sources of distortions in the standard Λ CDM cosmology. For the numbers given in the text, we use the best-fitting parameters from *Planck* for the TT,TE,EE + lowP dataset (Planck Collaboration et al. 2015b). Specifically, we use a flat model with $T_0 = 2.726$ K, $h = 0.6727$, $\Omega_c h^2 = 0.1198$, $\Omega_b h^2 = 0.02225$, $Y_p = 0.2467$ and $N_{\text{eff}} = 3.046$, with their standard meaning (Planck Collaboration et al. 2015b).

2.1 Reionization and structure formation

The first sources of radiation during reionization (Hu et al. 1994b), supernova feedback (Oh et al. 2003) and structure formation shocks (Sunyaev & Zeldovich 1972; Cen & Ostriker 1999; Refregier et al. 2000; Miniati et al. 2000) heat the intergalactic medium at low redshifts ($z \lesssim 10$), leading to a partial up-scattering of CMB photons, causing a Compton y -distortion (Zeldovich & Sunyaev 1969). Although this is the *largest* expected average distortion of the CMB caused within Λ CDM, its amplitude is quite uncertain and depends on the detailed structure and temperature of the medium, as well as

scaling relations (e.g., between halo mass and temperature). Several estimates for this contribution were obtained, yielding values for the total y -parameter at the level $y \approx \text{few} \times 10^{-6}$ (Refregier et al. 2000; Zhang et al. 2004; Hill et al. 2015; Dolag et al. 2015; De Zotti et al. 2015).

Following Hill et al. (2015), we will use a fiducial value of $y_{\text{re}} = 2 \times 10^{-6}$. This is dominated by the low mass end of the halo function and the signal should be detectable with *PIXIE* at more than $10^3 \sigma$. At this enormous significance, small corrections due to the high temperature ($kT_e \approx 1$ keV) of the gas become noticeable (Hill et al. 2015). The relativistic correction can be computed using the temperature moment method of SZpack (Chluba et al. 2012c, 2013) and it differs from the distortions produced in the early Universe. This correction should be detectable with *PIXIE* at $\approx 30 \sigma$ (Hill et al. 2015) and could teach us about the average temperature of the intergalactic medium, promising a way to solve the missing baryon problem. Both distortion signals are illustrated in Fig. 1.

2.2 Damping of primordial small-scale perturbations

The damping of small-scale fluctuations of the CMB temperature set up by inflation at wavelength $\lambda < 1$ Mpc causes another inevitable distortion of the CMB spectrum (Sunyaev & Zeldovich 1970a; Daly 1991; Barrow & Coles 1991; Hu et al. 1994a; Hu & Sugiyama 1994). While the idea behind this mechanism is quite simple, it was only recently rigorously described (Chluba et al. 2012b), allowing us to perform detailed computations of the associated distortion signal for different early universe models (Chluba et al. 2012b,a; Dent et al. 2012; Pajer & Zaldarriaga 2013; Khatri & Sunyaev 2013; Chluba & Grin 2013; Chluba 2013a; Clesse et al. 2014; Cabass et al. 2016). The distortion is sensitive to the amplitude and shape of the power spectrum at small scales (wavenumbers $1 \text{ Mpc}^{-1} \lesssim k \lesssim 2 \times 10^4 \text{ Mpc}^{-1}$) and thus provides a promising new way to constrain inflation.

For a given initial power spectrum of perturbations, the effective heating rate in general has to be computed numerically. However, at high redshifts the tight coupling approximation can be used to simplify the calculation. An excellent approximation for the effective heating rate is obtained with¹ (Chluba et al. 2012b; Chluba & Grin 2013)

$$\frac{d(Q/\rho_\gamma)}{dz} \approx 4A^2 \partial_z k_D^{-2} \int_{k_{\min}}^{\infty} \frac{k^4 dk}{2\pi^2} P_\zeta(k) e^{-2k^2/k_D^2}, \quad (1)$$

where $P_\zeta(k) = 2\pi^2 A_s k^{-3} (k/k_0)^{n_s-1+\frac{1}{2}n_{\text{run}} \ln(k/k_0)}$ defines the usual curvature power spectrum of scalar perturbations and k_D is the photon damping scale (Weinberg 1971; Kaiser 1983), which scales as $k_D \approx 4.048 \times 10^{-6} (1+z)^{3/2} \text{ Mpc}^{-1}$ early on. For adiabatic modes, we have a heating efficiency $A^2 \approx (1+4R_\nu/15)^{-2} \approx 0.813$, where $R_\nu \approx 0.409$ for $N_{\text{eff}} = 3.046$. The k -space integral is truncated at $k_{\min} \approx 0.12 \text{ Mpc}^{-1}$, which reproduces the full heating rate across the recombination era quite well (Chluba 2013a). With this we can directly compute the associated distortion using CosmoTherm (Chluba & Sunyaev 2012). The various isocurvature perturbations can be treated in a similar manner (e.g., Chluba & Grin 2013); however, in the standard inflation model these should be small. Tensor perturbations also contribute to the dissipation process; however, the associated heating rate is orders of magnitudes lower than for adiabatic modes even for very blue tensor power spectra and thus can be neglected (Ota et al. 2014; Chluba et al. 2015a).

¹ Here, we define the heating rate such that $\int_{k_{\min}}^{\infty} \frac{d(Q/\rho_\gamma)}{dz} dz > 0$.

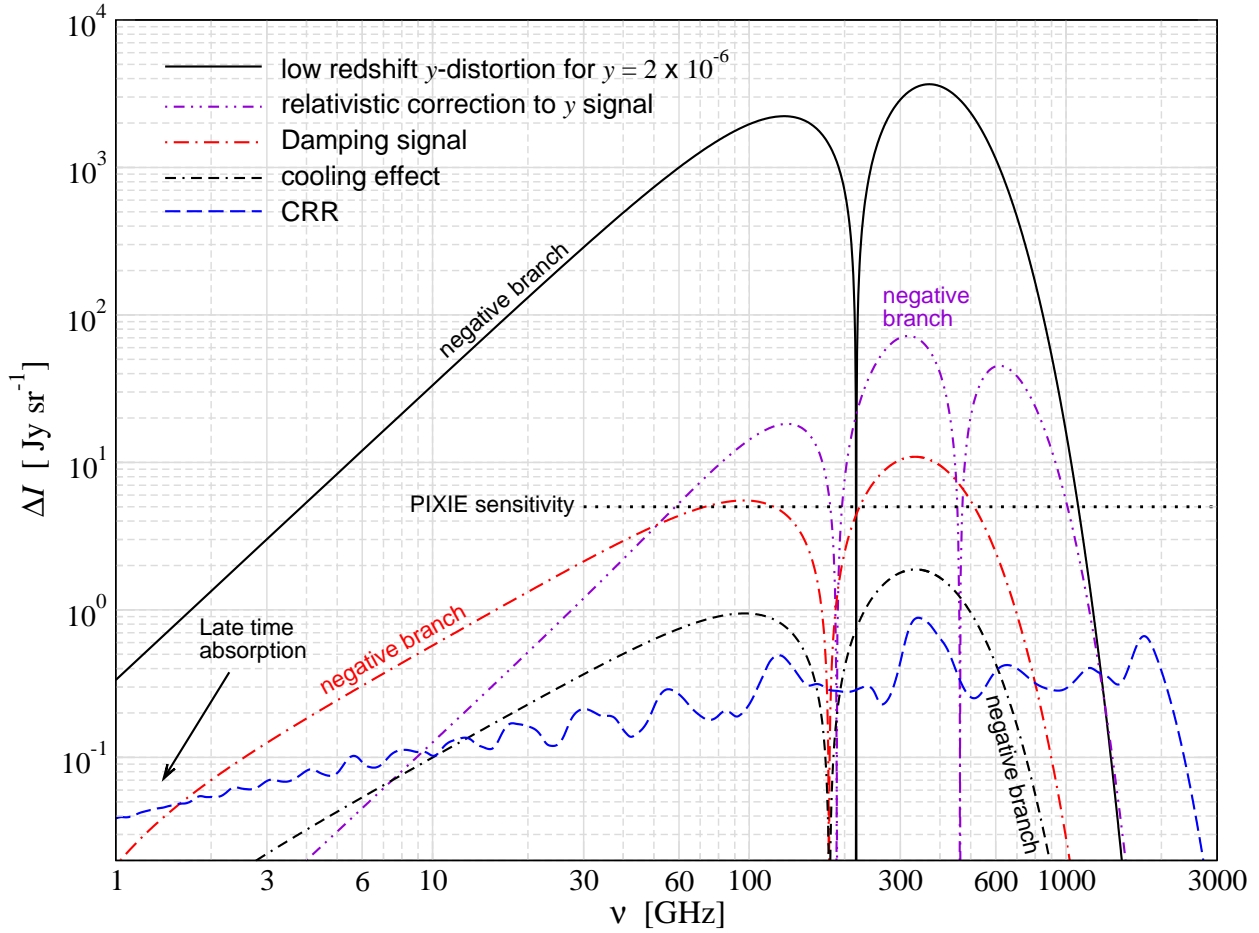


Figure 1. Comparison of several CMB monopole distortion signals produced in the standard Λ CDM cosmology. The low-redshift distortion created by reionization and structure formation is close to a pure Compton- y distortion with $y \approx 2 \times 10^{-6}$. Contributions from the hot gas in low mass haloes give rise to a noticeable relativistic temperature correction, which is taken from Hill et al. (2015). The damping and adiabatic cooling signals were explicitly computed using CosmoTherm (Chluba & Sunyaev 2012). The cosmological recombination radiation (CRR) was obtained with CosmoSpec (Chluba & Ali-Haïmoud 2016). The estimated sensitivity ($\Delta I_\nu \approx 5$ Jy/sr) of PIXIE is shown for comparison (dotted line). The templates will be made available at www.Chluba.de/CosmoTherm.

For $A_s = 2.207 \times 10^{-9}$, $n_s = 0.9645$ and $n_{\text{run}} = 0$ (Planck Collaboration et al. 2015b), we present the result in Fig. 1. The adiabatic cooling distortion (see Sect. 2.3) was simultaneously included. The signal is uncertain to within $\approx 10\%$ in Λ CDM (Sect. 3.3). The distortion lies between a μ - and y -distortion and is close to the detection limit of PIXIE. As we will see below (Sect. 4), with the current design the μ -distortion part of the signal should be seen at the level of $\approx 1.5\sigma$, which is in good agreement with earlier analysis (Chluba et al. 2012b; Chluba & Jeong 2014). A clear 5σ detection of this signal should be possible with ≈ 3.4 times higher sensitivity (Sect. 4). We will discuss various approximations for the damping signal below (Sect. 3), but simply performing a fit using μ , y and temperature shift (see Chluba & Jeong 2014, for explicit definitions of these spectral shapes), $\Delta = \Delta T/T_0$, we find $\mu_{\text{fit}} \approx 1.984 \times 10^{-8}$, $y_{\text{fit}} \approx 3.554 \times 10^{-9}$ and $\Delta_{\text{fit}} \approx -0.586 \times 10^{-9}$ with a non-vanishing residual at the level of 20% – 30%.

2.3 Adiabatic cooling for baryons

The adiabatic cooling of ordinary matter continuously extracts energy from the CMB photon bath by Compton scattering leading to another small but guaranteed distortion that directly depends on the

baryon density and helium abundance. The distortion is characterized by *negative* μ - and y -parameters at the level of $\approx \text{few} \times 10^{-9}$ (Chluba 2005; Chluba & Sunyaev 2012; Khatri et al. 2012). The effective energy extraction history is given by

$$\begin{aligned} \frac{d(Q/\rho_\gamma)}{dz} &= -\frac{3}{2} \frac{N_{\text{tot}} k T_\gamma}{\rho_\gamma (1+z)} \\ &\approx -\frac{5.71 \times 10^{-10}}{(1+z)} \left[\frac{(1-Y_p)}{0.7533} \right] \left[\frac{\Omega_b h^2}{0.02225} \right] \\ &\quad \times \left[\frac{(1+f_{\text{He}}+X_e)}{2.246} \right] \left[\frac{T_0}{2.726 \text{ K}} \right]^{-3} \quad (2) \end{aligned}$$

where $N_{\text{tot}} = N_H(1+f_{\text{He}}+X_e)$ is the number density of all thermally coupled baryons and electrons; $N_H \approx 1.881 \times 10^{-6} (1+z)^3 \text{ cm}^{-3}$ is the number density of hydrogen nuclei; $f_{\text{He}} \approx Y_p/4(1-Y_p) \approx 0.0819$ and $X_e = N_e/N_H$ is the free electron fraction, which can be computed accurately with CosmoRec (Chluba & Thomas 2011). For Planck 2015 parameters, the signal is shown in Fig. 1. It is uncertain at the $\approx 1\%$ level in Λ CDM (Sect. 3.3) and cancels part of the damping signal; however, it is roughly one order of magnitude weaker and cannot be separated at the currently expected level of sensitivity of next generation CMB spectrometers.

2.4 The cosmological recombination radiation

The cosmological recombination process is associated with the emission of photons in free-bound and bound-bound transitions of hydrogen and helium (Zeldovich et al. 1968; Peebles 1968; Dubrovich 1975). This causes a small distortion of the CMB and the redshifted recombination photons should be visible as the cosmological recombination radiation (CRR), a tiny spectral distortion ($\approx \text{nK-}\mu\text{K}$ level) present at mm to dm wavelength (for overview see Sunyaev & Chluba 2009). The amplitude of the CRR depends directly on the number density of baryons in the Universe. The helium abundance furthermore affects the detailed shape of the recombination lines. Finally, the line positions and widths depend on when and how fast the Universe recombined. The CRR thus provides an independent way to constrain cosmological parameters and map the recombination history (Chluba & Sunyaev 2008).

Several computations of this CRR have been carried out in the past (Rybicki & dell’Antonio 1993; Dubrovich & Stolyarov 1995, 1997; Kholupenko et al. 2005; Rubiño-Martín et al. 2006; Chluba & Sunyaev 2006; Chluba et al. 2007; Rubiño-Martín et al. 2008; Chluba & Sunyaev 2010; Chluba et al. 2010). These calculations were very time-consuming, taking a few days of supercomputer time for one cosmology (e.g., Chluba et al. 2007, 2010). This big computational challenge was recently overcome (Ali-Haïmoud 2013; Chluba & Ali-Haïmoud 2016), today allowing us to compute the CRR in about 15 seconds on a standard laptop using CosmoSpec² (Chluba & Ali-Haïmoud 2016). The *fingerprint* from the recombination era shows several distinct spectral features that encode valuable information about the recombination process (Fig. 1). Many subtle radiative transfer and atomic physics processes (e.g., Chluba et al. 2007; Chluba & Sunyaev 2010; Chluba & Thomas 2011; Ali-Haïmoud & Hirata 2011) are included by CosmoSpec, yielding the most detailed and accurate predictions of the CRR in the standard ΛCDM model to date. In ΛCDM , the CRR is uncertain at the level of a few percent, with the error being dominated by atomic physics (see Chluba & Ali-Haïmoud 2016).

The CRR is currently roughly ≈ 6 times below the estimated detection limit of *PIXIE* (cf. Fig. 1) and a detection from space will require several times higher sensitivity (Desjacques et al. 2015), which in the future could be achieved by experimental concepts similar to *PRISM* (André et al. 2014) or *Millimetron* (Smirnov et al. 2012). At low frequencies ($1\text{ GHz} \lesssim \nu \lesssim 10\text{ GHz}$), the significant spectral variability of the CRR may also allow us to detect it from the ground (Sathyanarayana Rao et al. 2015).

2.5 Superposition of blackbodies

It is well-known that the superposition of blackbodies with different temperatures no longer is a blackbody but exhibits a y -type spectral distortion (Zeldovich et al. 1972; Chluba & Sunyaev 2004; Stebbins 2007). It is precisely this effect that leads to the distortion caused by Silk-damping (e.g., Chluba et al. 2012b). To second order in the temperature fluctuations $\Delta_T = \Delta T/\bar{T} \ll 1$, the effective y -parameter is given by (cf., Chluba & Sunyaev 2004)

$$y = \frac{1}{2} \langle \Delta_T^2 \rangle, \quad (3)$$

where $\bar{T} = \langle T \rangle$ and the average can be related to any blackbody intensity mixing process. This can be i) Thomson scattering, ii) weighted averages of CMB *intensity* maps (e.g., due to spherical

harmonic decomposition) or iii) inevitable averaging inside the instrumental beam (Chluba & Sunyaev 2004). As mentioned above, i) occurs in the early Universe and also during reionization (e.g., Hu et al. 1994b; Chluba et al. 2012b) while ii) can occur as an *artefact* of the standard analysis of CMB intensity/antenna temperature maps, which can in principle be avoided by consistently converting to thermodynamic temperature at second order in Δ_T .

For the standard CMB temperature anisotropies, the beam averaging effect is tiny for angular resolution typical for today’s CMB imaging experiments (*Planck*, SPT, ACT, etc.) and should be completely negligible (Chluba & Sunyaev 2004). For a *PIXIE*-type experiment with beam $\approx 2^\circ$, the effect should be limited to $y \lesssim \text{few} \times 10^{-10} - 10^{-9}$ (Chluba & Sunyaev 2004); however, since high-resolution CMB temperature maps are available, this unavoidable effect can be taken into account very accurately.

The largest distortion due to the superposition of blackbodies with different temperatures is caused by the presence of the CMB dipole, with $\beta = v/c \approx (1.231 \pm 0.003) \times 10^{-3}$ (Hinshaw et al. 2009). Averaging the CMB intensity³ over the whole sky yields (Chluba & Sunyaev 2004)

$$y_d = \frac{\beta^2}{6} \approx (2.525 \pm 0.012) \times 10^{-7}. \quad (4)$$

with sky-averaged temperature dispersion $\langle [\beta \cos(\theta)]^2 \rangle = \beta^2/3$. The uncertainty, $\Delta y_0^d \approx 1.2 \times 10^{-9}$, in the contribution of the CMB dipole to the average y -parameter is a few times larger than the y -parameter induced by multipoles $\ell > 1$ (see below). One may also worry about higher order temperature terms from the dipole (Chluba & Sunyaev 2004), however, only even moments contribute, so that the next order correction averaged over the whole sky, $\langle [\beta \cos(\theta)]^4 \rangle \approx \beta^4/5 \approx (4.59 \pm 0.04) \times 10^{-13}$, is negligible, although it could still contribute noticeably in the far Wien tail ($\nu \gtrsim 1\text{ THz}$). We mention that in the presence of a primordial dipole, we would in addition obtain a y -parameter contribution $y_0^{\text{pb}} \approx \beta \Delta_{10} / \sqrt{12\pi}$, which is caused by aberration and Doppler boosting (Chluba 2011) and could reach $\approx 10^{-9}$. Here, Δ_{10} is the spherical harmonic coefficient of the primordial dipole along the direction of the CMB dipole.

Averaging the CMB intensity spectrum over the whole sky (after subtracting the CMB dipole spectrum), from the measured *Planck* temperature power spectrum (Planck Collaboration et al. 2015b) we find

$$y_{\text{sup}} = \sum_{\ell=2} \frac{(2\ell+1)C_\ell}{8\pi} \approx 8.23 \times 10^{-10}, \quad (5)$$

which is extremely close to an earlier estimate based on the theoretical CMB power spectrum (Chluba et al. 2012b). The uncertainty in this derived value is dominated by large-angle foreground residuals but is estimated to be below $\approx 1\%$. As this number is specific to our realization of the Universe and to our own location, it is *not* limited by cosmic variance. The CMB temperature is increased by $\Delta T \approx 4.49\text{ nK}$ due to the same effect.

We mention that the superposition of blackbodies of different temperatures has a slightly different physical effect than energy exchange through Compton scattering. In the latter case, energy is transferred from the electrons to the photons (assuming heating), such that photons are (partially) upscattered and afterwards *all* the energy is stored in the associated (y -type) distortion. For

² www.Chluba.de/CosmoSpec

³ We emphasize again that this distortion is *not* produced if the thermodynamic temperature, computed to second order in the fluctuations, was used.

the mixing of blackbodies, *no* energy exchange between photons and electrons is required (\leftrightarrow Thomson limit) and 2/3 of the energy stored by the original temperature fluctuations causes an increase for the average blackbody temperature. Thus, for a y -distortion created through the superposition of blackbodies one also finds an average temperature shift $\Delta T/\bar{T} = 2y_{\text{sup}}$ (Chluba et al. 2012b, 2015b; Inogamov & Sunyaev 2015). For the effect of the dipole this implies $\Delta T_d/T_0 = \beta^2/3$ caused by the superposition. However, another correction, $\Delta T_D/T_0 \approx -\beta^2/2$, arises from the Lorentz boost, so that the total temperature shift is $\Delta T = \Delta T_d + \Delta T_D = -T_0\beta^2/6 \approx -(0.688 \pm 0.003)\mu\text{K}$ (Chluba & Sunyaev 2004; Chluba 2011).

2.6 Dark matter annihilation

Today, cold dark matter is a well-established constituent of our Universe (Bennett et al. 2003; Planck Collaboration et al. 2014d, 2015b). However, the nature of dark matter is still unclear and many groups are trying to gather any new clue to help unravel this big puzzle (e.g., Adriani et al. 2009; Galli et al. 2009; CDMS II Collaboration et al. 2010; Zavala et al. 2011; Hütsi et al. 2011; Bringmann et al. 2012; Aslanyan et al. 2015). Similarly, it is unclear how dark matter was produced, however, within Λ CDM, the WIMP scenario provides one viable solution (e.g., Jungman et al. 1996; Bertone et al. 2005). In this case, dark matter should annihilate at a low level throughout the history of the Universe and even today.

For specific dark matter models, the level of annihilation around the recombination epoch is tightly constrained with the CMB anisotropies (Galli et al. 2009; Cirelli et al. 2009; Hütsi et al. 2009; Slatyer et al. 2009; Hütsi et al. 2011; Giesen et al. 2012; Diamanti et al. 2014; Planck Collaboration et al. 2015b). The annihilation of dark matter can cause changes in the ionization history around last scattering ($z \approx 10^3$), which in turn can lead to changes of the CMB temperature and polarization anisotropies (Chen & Kamionkowski 2004; Padmanabhan & Finkbeiner 2005; Zhang et al. 2006). Albeit significant dependence on the interaction of the annihilation products with the primordial plasma (Shull & van Steenberg 1985; Slatyer et al. 2009; Valdés et al. 2010; Galli et al. 2013; Slatyer 2016), the same process should lead to distortions of the CMB (McDonald et al. 2001; Chluba 2010; Chluba & Sunyaev 2012). The effective heating rate of the medium can be expressed as (see also Chluba 2013a)

$$\frac{d(Q/\rho_\gamma)}{dz} = f_{\text{ann}} \frac{N_{\text{H}}(z)(1+z)^{2+\lambda}}{H(z)\rho_\gamma(z)} \quad (6)$$

where $\lambda = 0$ for s-wave annihilation. Here, H denotes the Hubble factor and ρ_γ the CMB photon energy density. The annihilation efficiency, f_{ann} , captures all details related to the dark matter physics (e.g., annihilation cross section, mass, decay channels, etc.) and can be roughly taken as constant. For existing upper limits on f_{ann} , the distortion is well below the detection limit of *PIXIE* (Chluba & Sunyaev 2012; Chluba 2013a; Chluba & Jeong 2014). Using the latest constraints from *Planck*, we find the μ -distortion to be $\mu \lesssim \text{few} \times 10^{-10} - 10^{-9}$ (see Sect. 3.3). For s-wave annihilation scenarios, this limit ought to be rather conservative, and it is hard to imagine a much larger effect. However, spectral distortion measurements are sensitive to *all* energy release at $z \lesssim 2 \times 10^6$ and not only limited to around last scattering. Thus, searches for this small distortion could deliver an important test of the WIMP paradigm should any signature of dark matter annihilation be found through another probe. Possible coupling of WIMPs to the baryons or photons could further enhance the adiabatic cooling effect (Ali-Haïmoud et al. 2015), which could provide additional tests of the nature of dark matter especially for low dark matter masses.

2.7 Anisotropic CMB distortions

To close the discussion of different distortion signals, we briefly mention anisotropic (\leftrightarrow *spectral-spatial*) CMB distortions. Even in the standard Λ CDM cosmology, anisotropies in the spectrum of the CMB are expected. The largest source of anisotropies is due to the Sunyaev-Zeldovich effect caused by the hot plasma inside clusters of galaxies (Zeldovich & Sunyaev 1969; Sunyaev & Zeldovich 1980; Birkinshaw 1999; Carlstrom et al. 2002). The y -distortion power spectrum has already been measured directly by *Planck* (Planck Collaboration et al. 2014e, 2015d) and encodes valuable information about the atmospheres of clusters (e.g., Refregier et al. 2000; Komatsu & Seljak 2002; Diego & Majumdar 2004; Battaglia et al. 2010; Shaw et al. 2010; Munshi et al. 2013; Dolag et al. 2015). Similarly, the warm hot intergalactic medium contributes (Zhang et al. 2004; Dolag et al. 2015).

In the primordial Universe, anisotropies in the μ and y distortions are expected to be tiny (relative perturbations $\lesssim 10^{-4}$, e.g., see Pitrou et al. 2010) unless strong spatial variations in the primordial heating mechanism are expected (Chluba et al. 2012b). This could in principle be caused by non-Gaussianity of perturbations in the ultra-squeezed limit (Pajer & Zaldarriaga 2012; Ganc & Komatsu 2012; Biagetti et al. 2013; Emami et al. 2015), however, this is beyond Λ CDM cosmology and will not be considered further.

Another guaranteed anisotropic signal is due to Rayleigh scattering of CMB photons in the Lyman-series resonances of hydrogen around the recombination era (Yu et al. 2001; Lewis 2013). The signal is strongly frequency dependent, can be modeled precisely and may be detectable with future CMB imagers (e.g., *CORE+*) or possibly *PIXIE* at large angular scales (Lewis 2013). In a very similar manner, the resonant scattering of CMB photons by metals appearing in the dark ages (Loeb 2001; Zaldarriaga & Loeb 2002; Basu et al. 2004; Hernández-Monteagudo et al. 2007) or scattering in the excited levels of hydrogen during recombination (Rubiño-Martín et al. 2005; Hernández-Monteagudo et al. 2007) can lead to anisotropic distortions. To measure these signals, precise channel cross-calibration and foreground rejection is required.

Due to our motion relative to the CMB rest frame, the spectrum of the CMB dipole should also be distorted simply because the CMB monopole has a distortion (Danese & de Zotti 1981; Balashev et al. 2015). The signal associated with the large late-time y -distortion could be detectable with *PIXIE* at the level of a few σ (Balashev et al. 2015). Since for these measurements no absolute calibration is required, this effect will allow us to check for systematics. In addition, the dipole spectrum can be used to constrain monopole foregrounds (Balashev et al. 2015; De Zotti et al. 2015).

Finally, again due to the superposition of blackbodies (caused by the spherical harmonic expansion of the intensity map), the CMB quadrupole spectrum is also distorted, exhibiting a y -distortion related to our motion (Kamionkowski & Knox 2003; Chluba & Sunyaev 2004). The associated effective y -parameter is $y_Q = \beta^2/6 \approx (2.525 \pm 0.012) \times 10^{-7}$ and should be noticeable with *PIXIE* and future CMB imagers.

3 APPROXIMATIONS FOR THE DISTORTION SIGNALS

The primordial distortion signals that are caused by early energy release can be precisely computed using *CosmoTherm* (Chluba & Sunyaev 2012). However, for parameter estimation we will use Green's function method developed by Chluba (2013b). The results for different scenarios will be compared with more approximate but very simple estimates summarized in the next section.

3.1 Simple estimates for the μ - and y -parameters

To compute estimates for the μ - and y -parameters, several approximations have been discussed in the literature. Given the energy release history, $d(Q/\rho_\gamma)/dz$, they can all be compactly written as (e.g., Chluba 2013b; Chluba & Jeong 2014)

$$y = \frac{1}{4} \frac{\Delta\rho_\gamma}{\rho_\gamma} \Big|_y = \frac{1}{4} \int_0^\infty \mathcal{J}_y(z') \frac{d(Q/\rho_\gamma)}{dz'} dz' \quad (7a)$$

$$\mu = 1.401 \frac{\Delta\rho_\gamma}{\rho_\gamma} \Big|_\mu = 1.401 \int_0^\infty \mathcal{J}_\mu(z') \frac{d(Q/\rho_\gamma)}{dz'} dz' \quad (7b)$$

where $\Delta\rho_\gamma/\rho_\gamma|_y$ and $\Delta\rho_\gamma/\rho_\gamma|_\mu$ denote the effective energy release in the y - and μ -era, respectively. The individual distortion visibility functions, $\mathcal{J}_i(z)$, determine the differences between various existing approximations. The simplest approach assumes that the transition between μ and y occurs sharply at $z = z_{\mu y} \approx 5 \times 10^4$ and that no distortions are created at $z \gtrsim z_{th}$, where z_{th} is the thermalization redshift, which is given by (Burigana et al. 1991; Hu & Silk 1993a)

$$z_{th} \approx 1.98 \times 10^6 \left[\frac{(1 - Y_p/2)}{0.8767} \right]^{-2/5} \left[\frac{\Omega_b h^2}{0.02225} \right]^{-2/5} \left[\frac{T_0}{2.726 \text{ K}} \right]^{1/5}. \quad (8)$$

In this case, we have the simple approximation ('Method A')

$$\mathcal{J}_y(z) = \begin{cases} 1 & \text{for } z_{rec} \leq z \leq z_{\mu y} \\ 0 & \text{otherwise} \end{cases} \quad (9a)$$

$$\mathcal{J}_\mu(z) = \begin{cases} 1 & \text{for } z_{\mu y} \leq z \leq z_{th} \\ 0 & \text{otherwise.} \end{cases} \quad (9b)$$

For the estimates of y from early energy release, we will not include any contributions from after recombination, $z \lesssim 10^3 = z_{rec}$. These contributions will be attributed to the reionization y -parameter.

The next improvement is achieved by taking into account that the thermalization efficiency does not abruptly vanish at $z \approx z_{th}$, but that even at $z > z_{th}$ a small μ -distortion is produced (Sunyaev & Zeldovich 1970b; Danese & de Zotti 1982; Burigana et al. 1991; Hu & Silk 1993a). With this we have ('Method B')

$$\mathcal{J}_y(z) = \begin{cases} 1 & \text{for } z_{rec} \leq z \leq z_{\mu y} \\ 0 & \text{otherwise} \end{cases} \quad (10a)$$

$$\mathcal{J}_\mu(z) = \begin{cases} \mathcal{J}_{bb}(z) & \text{for } z_{\mu y} \leq z \\ 0 & \text{otherwise.} \end{cases} \quad (10b)$$

where $\mathcal{J}_{bb}(z) \approx e^{-(z/z_{th})^{5/2}}$ is the *distortion visibility function*.⁴

The next simple approximations also include the fact that the transition between μ and y distortions is not abrupt at $z \approx z_{\mu y}$. The distortion around this redshift is mostly given by a superposition of μ and y , with a smaller correction in form of the residual (r -type) distortion, which can be modeled numerically. By simply determining the best-fitting approximation to the distortion Green's function using only μ and y one can write (Chluba 2013b)

$$\mathcal{J}_y(z) \approx \begin{cases} \left(1 + \left[\frac{1+z}{6 \times 10^4} \right]^{2.58} \right)^{-1} & \text{for } z_{rec} \leq z \\ 0 & \text{otherwise} \end{cases} \quad (11a)$$

$$\mathcal{J}_\mu(z) \approx \mathcal{J}_{bb}(z) \left[1 - \exp \left(- \left[\frac{1+z}{5.8 \times 10^4} \right]^{1.88} \right) \right]. \quad (11b)$$

⁴ Refined approximation for the distortion visibility function have been discussed (Khatri & Sunyaev 2012b; Chluba 2014), but once higher accuracy is required it is easier to directly use the Green's function method, such that we do not go into more details here.

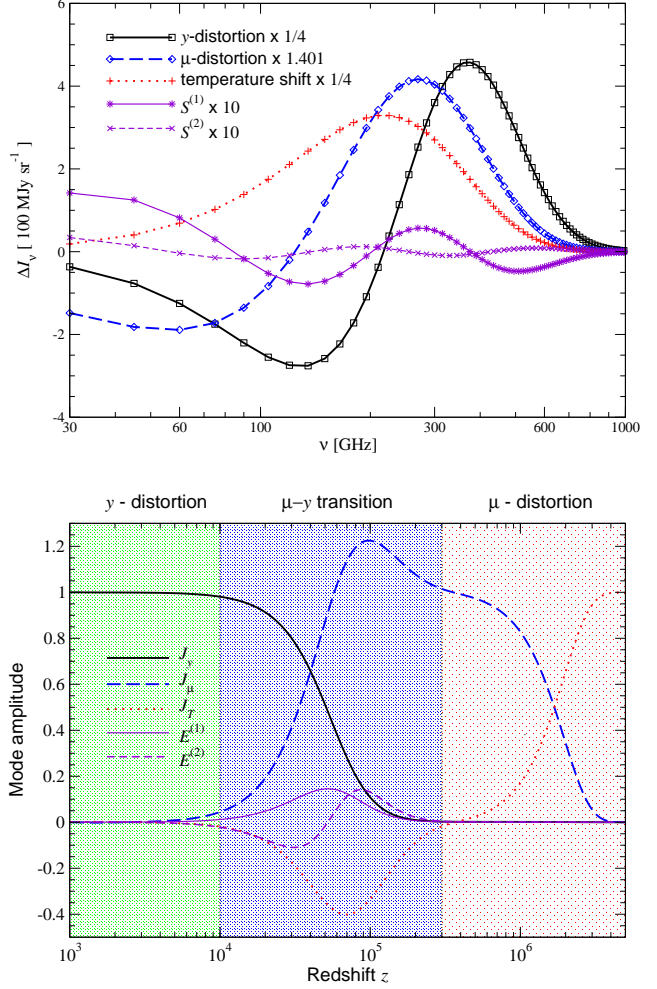


Figure 2. Principal component decomposition for *PIXIE*-like setting ($\{\nu_{min}, \nu_{max}, \Delta\nu\} = \{30, 1000, 15\}$ GHz). – Upper panel: first two residual distortion eigenmodes, $S^{(k)}$, in comparison with the spectral shapes of temperature shift, μ and y -distortions. We scaled the templates by convenient factors to make them comparable in amplitude. – Lower panel: associated energy release eigenmodes, $E^{(k)}$, and visibilities, J_i , of temperature shift, μ and y -distortions. The figures were adapted from Chluba & Jeong (2014).

We shall refer to this as ‘Method C’ and only represents the exact proportions of μ and y to $\approx 10\% - 20\%$ precision. To ensure full energy conservation (no leakage of energy to the r -distortion), instead one can use $\mathcal{J}_\mu(z) \approx [1 - \mathcal{J}_y(z)] \mathcal{J}_{bb}(z)$ (‘Method D’).

All the above expressions give slightly different results for the expected distortion μ and y -parameters. Below we will compare them with the more accurate distortion principal component decomposition (Chluba & Jeong 2014), which optimizes the representation when simultaneously estimating μ , y and $\Delta = \Delta T/T_0$. At the same time, these approximations allow one to quickly estimate the expected distortion signals and their dependence on different parameters, which can be useful for order of magnitude work. We will see that a simple interpretation of the distortion in terms of μ and y derived in this way differs slightly from what future measurements will recover (Sect. 3.3). Specifically, due to the uncertainty in the value of the CMB monopole, the projections of the distortion signals on to μ are underestimated by $\approx 20\% - 30\%$ (Table 1).

Table 1. Comparison of distortion parameters for various methods and types of scenarios with cosmological parameters based on the *Planck* 2015 TT,TE,EE+lowP results (Planck Collaboration et al. 2015b). The uncertainties for the predictions in the dissipation scenarios are dominated by the uncertainties in the power spectrum parameters. Assuming standard BBN ($Y_p = 0.2467$), for the adiabatic cooling distortion the small uncertainty is dominated by that of the baryon density. This contribution to the total distortion is also included in the values given for the dissipation scenarios. For the annihilation scenario, we assumed s-wave annihilation for a Majorana dark matter particle using $p_{\text{ann}} < 4.1 \times 10^{-28} \text{ cm}^3 \text{ sec}^{-1} \text{ GeV}^{-1}$ (Planck Collaboration et al. 2015b) with $f_{\text{ann}} = (\rho_c^2 c^4 \Omega_{\text{cdm}}^2 / N_{\text{H},0}) p_{\text{ann}} \approx 8.5 \times 10^3 \text{ eV sec}^{-1} p_{\text{ann}} / [\text{cm}^3 \text{ sec}^{-1} \text{ GeV}^{-1}]$. All quoted error bars are for 68% c.l. and the central values are medians.

	Parameter	Dissipation I	Dissipation II	Adiabatic cooling	Annihilation (s-wave)
	$\ln(10^{10} A_s)$	3.094 ± 0.034	3.103 ± 0.036	–	–
	n_s	0.9645 ± 0.0049	0.9639 ± 0.0050	–	–
	n_{run}	0	-0.0057 ± 0.0071	–	–
	$100 \Omega_b h^2$	2.225 ± 0.016	2.229 ± 0.017	2.225 ± 0.016	2.225 ± 0.016
	f_{ann}	–	–	–	$< 3.5 \times 10^{-24} \text{ eV sec}^{-1}$ (95% c.l.)
Method A	$y/10^{-9}$	$3.67^{+0.17}_{-0.17}$	$3.53^{+0.25}_{-0.23}$	$-0.532^{+0.003}_{-0.003}$	< 0.091
	$\mu/10^{-8}$	$1.72^{+0.13}_{-0.12}$	$1.31^{+0.52}_{-0.38}$	$-0.296^{+0.002}_{-0.002}$	< 0.062
Method B	$y/10^{-9}$	$3.67^{+0.18}_{-0.17}$	$3.54^{+0.25}_{-0.23}$	$-0.532^{+0.003}_{-0.003}$	< 0.091
	$\mu/10^{-8}$	$1.62^{+0.12}_{-0.11}$	$1.27^{+0.49}_{-0.36}$	$-0.277^{+0.002}_{-0.002}$	< 0.058
Method C	$y/10^{-9}$	$3.83^{+0.19}_{-0.18}$	$3.66^{+0.28}_{-0.26}$	$-0.558^{+0.003}_{-0.003}$	< 0.097
	$\mu/10^{-8}$	$1.71^{+0.12}_{-0.12}$	$1.34^{+0.48}_{-0.36}$	$-0.290^{+0.002}_{-0.002}$	< 0.061
Method D	$y/10^{-9}$	$3.83^{+0.19}_{-0.18}$	$3.66^{+0.29}_{-0.26}$	$-0.558^{+0.003}_{-0.003}$	< 0.097
	$\mu/10^{-8}$	$1.54^{+0.11}_{-0.11}$	$1.18^{+0.46}_{-0.33}$	$-0.263^{+0.001}_{-0.001}$	< 0.055
PCA	$y/10^{-9}$	$3.63^{+0.17}_{-0.17}$	$3.49^{+0.26}_{-0.23}$	$-0.527^{+0.003}_{-0.003}$	< 0.091
	$\mu/10^{-8}$	$2.00^{+0.14}_{-0.13}$	$1.59^{+0.54}_{-0.40}$	$-0.334^{+0.002}_{-0.002}$	< 0.070
	$\mu_1/10^{-8}$	$3.81^{+0.22}_{-0.21}$	$3.39^{+0.58}_{-0.49}$	$-0.587^{+0.003}_{-0.003}$	< 0.12
	$\mu_2/10^{-9}$	$-1.19^{+0.22}_{-0.20}$	$-2.79^{+2.05}_{-1.53}$	$-0.051^{+0.001}_{-0.001}$	< 0.046

3.2 Distortion principal component decomposition

The approximations given in the previous section are all based on simple analytical considerations. However, the CMB spectrum is given by a superposition of μ , y and r distortions as well as the CMB monopole temperature. The situation is further complicated by the presence of large foregrounds. Also, when considering instrumental effects (number of channels, upper and lower frequency channel and frequency resolution, etc.), different spectral shapes cannot be uniquely separated and project on to each other. In this case, a principal component analysis (PCA) helps parametrizing the expected distortion shapes with a small number of distortion parameters, ranked by their expected signal to noise ratio.

Considering experimental setting similar to *PIXIE*, this decomposition was carried out previously (Chluba & Jeong 2014), identifying new distortion parameters, μ_k , to describe the r -type distortion. Since a minimal distortion parameter estimation will include μ , y and $\Delta = \Delta T/T_0$, the r -type distortion is defined such that none of the μ_k correlated with any of these. For the technical details we refer to Chluba & Jeong (2014), but the primordial distortion signal in each frequency bin can then be decomposed as

$$\Delta I_i = \Delta I_i^T + \Delta I_i^\mu + \Delta I_i^y + \Delta I_i^R \quad (12a)$$

$$\Delta I_i^R \approx \sum_k S_i^{(k)} \mu_k, \quad (12b)$$

where ΔI_i^T , ΔI_i^μ and ΔI_i^y correspond to the spectral shapes of a temperature shift, μ - and y -distortions, respectively; ΔI_i^R describes the r -type distortion, where μ_k and $S_i^{(k)}$ are the amplitude and distortion signal of the k^{th} eigenmode, respectively (see Fig. 2).

The signal eigenmodes, $S_i^{(k)}$, are associated with a set of energy release eigenvectors, $E^{(k)}$, in discretized redshift space, which are normalized as $E^{(k)} \cdot E^{(l)} = \delta_{kl}$. Any given energy-release history, $Q(z) = d(Q/\rho_\gamma)/d \ln z$, can then be written as

$$Q \approx \sum_k E^{(k)} \mu_k, \quad (13)$$

where $Q = (Q(z_0), Q(z_1), \dots, Q(z_n))^T$ is the energy-release vector of $Q(z)$ in different redshift bins. By construction, the eigenvectors, $E^{(k)}$, span an ortho-normal basis, while all $S^{(k)}$ only define an orthogonal basis (generally $S^{(k)} \cdot S^{(l)} \geq \delta_{kl}$). The mode amplitudes are then obtained as simple scalar product, $\mu_k = E^{(k)} \cdot Q$. The eigenmodes are ranked by their signal-to-noise, such that modes with larger k contribute less to the signal. In a similar way, we can write $\mu = 1.401 J_\mu \cdot Q$, $4y = J_y \cdot Q$ and $4\Delta T/T_0 = J_T \cdot Q$, where the J_i vectors play the role of effective visibilities, like in the integral versions, Eq. (7). The first few energy-release eigenmodes and E^i are shown in Fig. 2. We note that again only heating at $z \geq 10^3$ is included in the estimates of the distortion parameters. This can underestimate the y -parameter at the $\approx 10\%$ level (see Sect. 3.3).

Although in terms of simple scattering physics, distortion signals created by energy release at $z \lesssim \text{few} \times 10^5$ should deviate from a simple μ -distortion (Hu 1995; Chluba & Sunyaev 2009, 2012; Khatri & Sunyaev 2012a; Chluba 2013b), even at lower redshift a non-vanishing additional projection on to μ is found (Chluba & Jeong 2014), as reflected by an increase of J^μ around $z \approx 10^5$ (see Fig. 2). This enhances the recovered value of μ when the parameter estimation problem for μ , y and Δ is solved (see below), an effect that is mainly due to the fact that the average CMB temperature has to be determined simultaneously.

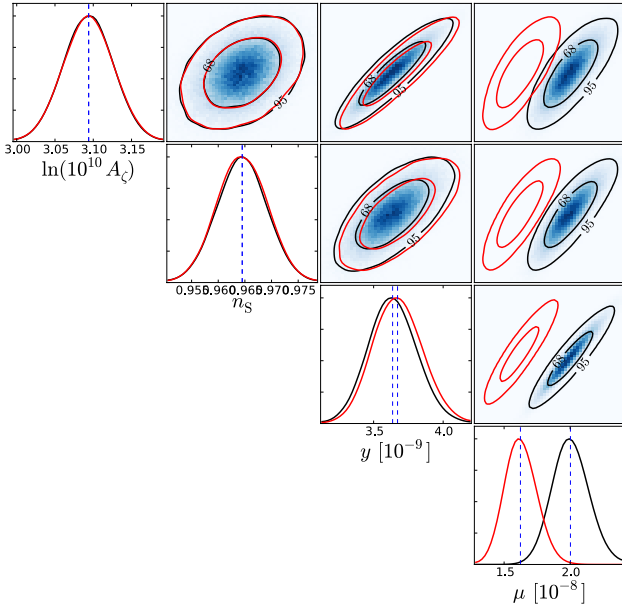


Figure 3. Comparison of the posterior distributions for the dissipation scenario I (Table 1) obtained with method B (red contours) and the PCA (black contours). The vertical lines indicate the mean values. Method B predicts lower values for μ than the distortion eigenmode analysis.

We immediately mention that one alternative approach, which could mitigate the above problem, could be to determine the average CMB temperature using the integral properties of the μ , y and r -distortions. Since these are created by a scattering process, the number density of photons should not change. Thus, determining the effective temperature of the CMB by computing the total photon number density ($N_\gamma \propto T_\gamma^3$) from the measured spectrum, the distortions would not contribute under idealized assumptions. However, this procedure is not expected to work well for discretized versions of the spectra. It is furthermore complicated by the presence of foregrounds and the possibility of non-standard processes that can actually lead to non-trivial photon injection (Chluba 2015). Finally, the r -distortion parameters would no longer remain uncorrelated, so that we do not explore this avenue any further.

3.3 Results from the different methods

We are now in the position to explicitly compute the μ - and y -parameters for the different distortion scenarios discussed above. With the PCA, we are furthermore able to obtain the eigenmode amplitudes, μ_1 and μ_2 . We stop at the second residual distortion eigenmode, since observing μ_2 is already very futuristic for standard scenarios. We also mention that the values for y are only used as a comparison, since the y -distortion from the low-redshift Universe is much larger in all cases.

In our estimates, we include the measurement uncertainties for the relevant Λ CDM parameters (Planck Collaboration et al. 2015b). For the dissipation scenarios, these are mainly related to the power spectrum parameters, while for the adiabatic cooling distortion it is the baryon density (assuming standard BBN). The results are summarized in Table 1. For the dissipation scenarios, we obtained the error estimates by using the relevant covariance matrix for the *Planck* data, while the error for the adiabatic cooling effect was directly estimated using Gaussian error propagation.

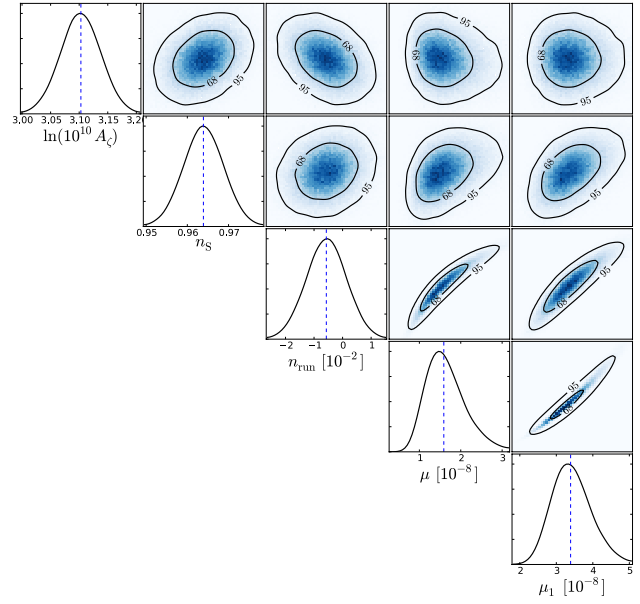


Figure 4. Posterior distributions for the dissipation scenario II (Table 1) obtained with the PCA. We omitted y as its posterior remains fairly Gaussian. The vertical lines indicate the mean values.

Table 2. Explicit projections of the full CosmoTherm output using the distortion eigenmodes for *PIXIE*-like settings. The last column also gives the estimates 1σ error for *PIXIE* in its current design (Chluba & Jeong 2014), which degrades quickly for the μ_k . In parenthesis, we show estimates for the expected significance in terms of distortion measurements.

Parameter	Dissipation I	Adiabatic cooling	<i>PIXIE</i> 1σ
$y/10^{-9}$	3.54 ($\approx 3.0\sigma$)	-0.623 ($\approx 0.5\sigma$)	1.20
$\mu/10^{-8}$	2.00 ($\approx 1.5\sigma$)	-0.334 ($\approx 0.2\sigma$)	1.37
$\mu_1/10^{-8}$	3.82 ($\approx 0.3\sigma$)	-0.588 ($\approx 0.04\sigma$)	14.8
$\mu_2/10^{-9}$	-1.18 ($\approx 0.0\sigma$)	-0.054 ($\approx 0.0\sigma$)	761

For the y -parameter estimates, methods A and B are equivalent and give results which are quite close to those of the PCA, which should be considered the most precise representation of what would be recovered in a distortion analysis. The methods C and D are also equivalent, but overestimate the y -parameter by $\approx 5\% - 10\%$ in comparison to the PCA. The recovered error bars for all methods are very comparable. For the μ -parameter, all methods are slightly different. The PCA always gives 20%–30% larger values. The best agreement with the PCA is achieved by methods A and C. Again all methods give very similar estimates for the expected errors.

In Fig. 3, we highlight the differences in the predicted y and μ -parameters for the dissipation scenario I obtained with method B and the PCA⁵. The errors are dominated by uncertainties in the power spectrum parameters. The result for y agrees quite well, while the result for μ is biased low by $\approx 2.6\sigma$ with method B, a difference that needs to be taken into account when interpreting

⁵ The figure was obtained using the Markov Chain Monte Carlo (MCMC) tool of the Greens software package (Chluba 2013b) available at www.Chluba.de/CosmoTherm.

future distortion measurements. The result from method B is very close to what was recently discussed in Cabass et al. (2016) for μ .

In Fig. 4, we show the posterior for dissipation scenario II (see Table 1). This is no longer a Λ CDM case, as for the standard inflation model running is negligible. However, it illustrates how well *Planck* data might constrain running and we will return to this case below when forecasting spectral distortion constraints. While in the case without running the posteriors for the distortion parameters remained fairly Gaussian, when including running those for μ , μ_1 and μ_2 become non-Gaussian. Since the *Planck* data prefers slightly negative running, implying less power at small scales, the median for μ decreases. Due to the long lever arm, small changes in n_{run} have a large effect on μ and μ_1 , so that their uncertainties increase significantly relative to the case without running (see Table 1). Conversely, this means that distortion measurements have constraining power in particular for n_{run} (e.g., Chluba et al. 2012b). Again, the expected recovered value for μ is slightly larger than what Cabass et al. (2016) find, whose central value is more close to that of methods A-C. However, in this case the significance of the bias is only $\approx 1\sigma$ due to increased uncertainty in the prediction.

3.4 Distortion parameters for full CosmoTherm outputs

We mention that by explicitly using the output from CosmoTherm for the dissipation scenario I and the adiabatic cooling case we find values summarized in Table 2. We can see that the agreement is excellent in comparison with the Green’s function projections that were used for the results presented in Table 1. The differences are mainly noticeable for the y -parameters, but even there they are $\lesssim 10\%$. The main reason for the difference is because with CosmoTherm we include the adiabatic cooling effect all the way to redshift $z = 200$, while in the Green’s function approximation we stop at $z = 10^3$. This gives another $y \approx -0.1 \times 10^{-9}$ correction, which one can simply add by hand. It is possible to improve this in the code, but since this is not distinguishable from the much larger y -distortion created at lower redshifts, we neglect it. We mention that we include part of the cosmology-dependence of the Green’s function, but at low frequencies this is only approximate.

4 FORECAST FOR PIXIE-LIKE EXPERIMENTS

We now discuss the prospects for detecting the different distortion signals. First of all, the y -parameter contributions are all insignificant compared to the y -parameter caused by low-redshift processes (Sect. 2.1). Although in terms of sensitivity, the contributions summarized in Table 1 are significant at the level of a few σ for *PIXIE* in its current design, these cannot be separated and are thus not discussed further (see Chluba 2013a; Chluba & Jeong 2014).

The μ -distortion amplitude for the dissipation scenario I is detectable at the level of $\approx 1.45\sigma$ (see also Chluba & Jeong 2014). This is a factor of ≈ 3.4 short of a clear $\approx 5\sigma$ detection of the standard Λ CDM signal (cf., Chluba et al. 2012b). One simple improvement in the sensitivity is achieved by halving the number of channels. For a Fourier Transform Spectrometer (FTS), such as in *PIXIE*, this improves the detection limits by a factor of $\approx \sqrt{2}$, since about twice as much time can be spent on each sample and but the total number of collected photons remains the same⁶. However, this also reduces the number of frequency channels in the CMB

regime and thus degrades our ability to reject foregrounds, requiring a more detailed optimization. Similarly, changes in the distribution of channels could improve the performance of *PIXIE*, but also call for a more careful analysis of foreground effects. Another way to improve the sensitivity is by extending the mission duration or by changing the time spent on spectral distortions versus B -mode science (Kogut et al. 2011; Chluba 2013a). Thus, factors of a few improvement in the raw spectral sensitivity seem to be within reach of current technology, although ultimate limitations by foregrounds need to be addressed carefully (Sect. 4.1).

One interesting question is at what effective sensitivity can a spectral distortion measurement confirm Λ CDM assuming the simplest slow-roll inflation model (see Baumann 2009, for review), which predicts $n_{\text{run}} \approx -\frac{1}{2}(n_s - 1)^2 \approx 6 \times 10^{-4}$ (Starobinsky 1980). To answer this, we assume a fiducial model for the small-scale power spectrum as in dissipation scenario I, which gives $\mu = 2.0 \times 10^{-8}$. However, we then compute the posterior assuming *Planck* constraints for the case with running. Adding spectral distortions should then pull the best-fitting solution closer to $n_{\text{run}} \approx 0$. We also add a large y -distortion signal⁷ $y = 2 \times 10^{-6}$ and a small shift in the CMB monopole temperature. Both parameters are estimated simultaneously with the power spectrum parameters using the MCMC tool of the Greens software package.

In Fig. 5, we illustrate this aspect for two channel sensitivities. Derived combined parameter constraints are summarized in Table 3. For the fiducial sensitivity of *PIXIE*, adding spectral distortions does not improve the constraints on power spectrum parameters significantly. For ≈ 3.4 times higher channel sensitivity, we find an $\approx 4.5\sigma$ detection of μ in terms of the uncertainty of the distortion measurement and a factor of $\approx 1.4 - 1.5$ improvement of the error on n_{run} , which starts to move towards the Λ CDM value. The uncertainties in the values of A_s and n_s are not improved much (see Fig. 5). At 10 times the sensitivity of *PIXIE*, which is similar to the spectrometer of the *PRISM* concept (André et al. 2014), the constraints are further tightened by adding spectral distortions, reducing the error on n_{run} by a factor of ≈ 3 over *Planck* alone. We also find an $\approx 15\sigma$ detection of the μ -distortion parameter and a marginal $\approx 2.6\sigma$ detection of μ_1 from distortions alone in this case. This sensitivity would furthermore make the CRR detectable at the level of a few σ (Desjacques et al. 2015).

In the near future, ground-based observations (Stage-IV CMB) in combination with the upcoming spectroscopic galaxy surveys, eBOSS and DESI, aim at improving limits on n_{run} by factors of a few (Abazajian et al. 2015a). One other target is to obtain improved constraints on neutrino physics (Abazajian et al. 2015b). As the μ -distortion from the dissipation scenario is mostly sensitive to n_{run} , adding spectral distortion measurements could help improving these limits by alleviating some existing degeneracies. However, enhanced versions of *PIXIE* are required in this case.

We highlight that the small-scale damping process is the dominant source of μ -distortions in Λ CDM. This implies that any significant departure from the expected signal (Table 2) inevitably points towards new physics. If the signal is much lower, then the small-scale CMB power spectrum, around wavenumbers $k \approx 740 \text{ Mpc}^{-1}$, where most of the μ -signal is created (see Emami et al. 2015, for illustration), either has a much lower amplitude (Chluba et al.

⁶ The effective channel sensitivity improves by a factor of 2, but half the number of channels are available to constrain the distortions so that overall only $\approx \sqrt{2}$ is gained (compare Kogut et al. 2011).

⁷ The uncertainty in the value of y from low redshifts removes about 2/3 of the constraining power of the dissipation signal. Without this large ‘foreground’ one would achieve a factor of ≈ 1.6 improvement of the constraint on n_{run} with *PIXIE* in its default setup already.

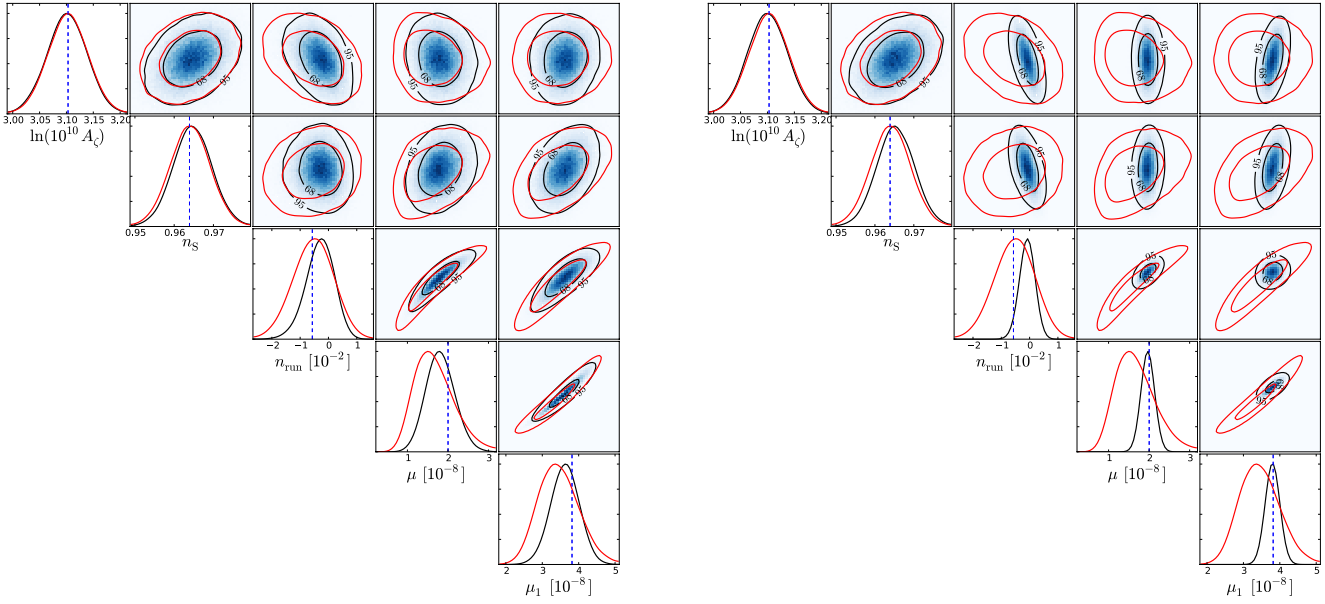


Figure 5. Posteriors for different combinations of data sets. In both panels, the red lines indicate the *Planck* TT,TE,EE+lowP+*PIXIE* (\equiv basically like without *PIXIE*) constraints for the extended model with running. The black contours show the *Planck*+3.4 \times *PIXIE* (left panel) and *Planck*+10 \times *PIXIE* (right panel) constraints. Vertical lines indicate the fiducial values for each data set. Adding spectral distortions helps diminishing the uncertainty in the values of n_{run} by a factor of ≈ 3 for *Planck*+10 \times *PIXIE*.

Table 3. Improvement of constraints on the small-scale power spectrum by combining *Planck* with a *PIXIE*-like experiment for different channel sensitivities. For the spectral distortion parameters, we also show the effective significance of the signal with respect to the spectral distortion measurement. The distortion amplitude μ_2 remained undetectable ($\lesssim 0.02\sigma$) with distortions alone and thus remains a *derived* parameter even for 10 \times *PIXIE* sensitivity. In the last column we show the *Planck* Λ CDM values for comparison.

Parameter	<i>Planck</i> alone	+ <i>PIXIE</i>	+3.4 \times <i>PIXIE</i>	+10 \times <i>PIXIE</i>	<i>Planck</i> Λ CDM values
$\ln(10^{10} A_s)$	$3.103^{+0.036}_{-0.036}$	$3.103^{+0.037}_{-0.037}$	$3.101^{+0.037}_{-0.037}$	$3.100^{+0.036}_{-0.036}$	$3.094^{+0.034}_{-0.034}$
n_s	$0.9639^{+0.0050}_{-0.0050}$	$0.9640^{+0.0050}_{-0.0050}$	$0.9647^{+0.0049}_{-0.0048}$	$0.9653^{+0.0048}_{-0.0047}$	$0.9645^{+0.0049}_{-0.0049}$
$10^3 n_{\text{run}}$	$-5.7^{+7.1}_{-7.1}$	$-5.2^{+6.9}_{-7.2}$	$-2.8^{+4.6}_{-5.1}$	$-0.81^{+2.4}_{-2.5}$	0
$\mu/10^{-8}$	$1.59^{+0.54}_{-0.40}$	$1.62^{+0.55}_{-0.42}$ (1.2 σ)	$1.81^{+0.36}_{-0.33}$ (4.5 σ)	$1.993^{+0.053}_{-0.053}$ (15 σ)	$2.00^{+0.14}_{-0.13}$
$\mu_1/10^{-8}$	$3.39^{+0.58}_{-0.49}$	$3.43^{+0.58}_{-0.52}$ (0.23 σ)	$3.63^{+0.38}_{-0.38}$ (0.83 σ)	$3.819^{+0.044}_{-0.044}$ (2.6 σ)	$3.81^{+0.22}_{-0.20}$
$\mu_2/10^{-9}$	$-2.79^{+2.05}_{-1.53}$	$-2.69^{+2.08}_{-1.61}$ (0 σ)	$-2.02^{+1.42}_{-1.31}$ (0 σ)	$-1.28^{+0.43}_{-0.43}$ (0 σ)	$-1.19^{+0.22}_{-0.20}$

2012b,a), or an enhanced cooling process through the coupling of another non-relativistic particle to the CMB is required (e.g., Ali-Haïmoud et al. 2015). Conversely, if the μ -distortion signal is much larger than expected, then the small-scale power spectrum could be strongly enhanced, possibly containing a localized feature (Chluba et al. 2012a, 2015b), or another heating mechanism (e.g., a decaying particle Hu & Silk 1993b; Chluba & Sunyaev 2012; Chluba 2013a; Dimastrogiovanni et al. 2015) has to be at work. Thus, spectral distortions provide a powerful new avenue for testing Λ CDM cosmology without purely relying on an extrapolation from large ($k \lesssim 1 \text{ Mpc}^{-1}$) to small scales ($1 \text{ Mpc}^{-1} \lesssim k \lesssim \text{few} \times 10^4 \text{ Mpc}^{-1}$).

4.1 Importance of refined foreground modeling

It is clear that for the success of spectral distortion measurements, the name of the game will be foregrounds. The biggest challenge is that, aside from the large y -distortion introduced at late times, all known foregrounds are orders of magnitudes larger than the pri-

mordial signals. This means that tiny effects related to the spectral and spatial variation of the foreground signals need to be taken into account. Ways to tackle this problem are i) to measure the spectrum in as many individual channels as possible, ideally with high angular resolution and sensitivity, and ii) to exploit synergies with other future or existing datasets to inform the modeling of averaged signals. In both cases, refined modeling of the foregrounds with extended parametrizations are required to capture the effects of averaging of spatially varying components across the sky.

An FTS concept like *PIXIE* pushes us into a qualitatively different regime in terms of its spectral capabilities, where instead of playing with a few channels we have a few hundred at our disposal. Most of these channels are at high frequencies ($\nu \gtrsim 1 \text{ THz}$), above the CMB bands and can be used to subtract the dust and cosmic infrared background components at lower frequencies (Kogut et al. 2011). Simple, commonly used two-temperature modified black-body spectra (e.g., Finkbeiner et al. 1999) will not provide suffi-

cient freedom to capture all relevant properties of the averaged dust spectrum. Existing maps from *Planck* (e.g., Planck Collaboration et al. 2014a, 2015a) can be used to estimate the effect of spatial variations of the dust temperature across the sky. Similar to the superposition of blackbodies with varying temperature (Sect. 2.5), this will cause new spectral shapes because of the i) *beam average* and ii) *all-sky averaging*, which need to be captured by extended foreground parametrizations (Chluba et al., 2016, in preparation). The associated parameters have to be directly determined in the distortion measurement, as existing data are not expected to provide sufficient information down to the noise level of experiments like *PIXIE*, but can be used to guide the modeling and parametrization.

Similar comments apply to the modeling of the synchrotron and free-free components at low frequencies. Albeit spectrally quite smooth, the superposition of spatially varying power-law spectra, $I_\nu \approx A_0 (\nu/\nu_0)^\alpha$ [where I_ν denotes the intensity], causes new spectral shapes that depend on *moments* of the underlying distribution functions. The common addition of curvature to the spectral index, $I_\nu \approx A_0 (\nu/\nu_0)^{\alpha + \frac{1}{2}\beta \ln(\nu/\nu_0)}$ (e.g., compare Remazeilles et al. 2015), is too restrictive. Extending the list of curvature parameters,

$$I_\nu^p \approx A_0 (\nu/\nu_0)^{\alpha + \frac{1}{2}\beta \ln(\nu/\nu_0) + \frac{1}{6}\gamma \ln^2(\nu/\nu_0) + \frac{1}{24}\delta \ln^3(\nu/\nu_0) + \dots}, \quad (14)$$

can be shown to capture all the new degrees of freedom for the superposition of power-law spectra, although this generalization does not have the best convergence properties (Chluba et al., 2016, in preparation). In Eq. (14), the coefficients α , β , γ and δ are directly related to the aforementioned moments of the spectral index distribution functions. These have to be determined with the distortion measurement, while external data sets (e.g., C-BASS, Irfan et al. 2015) can likely only be used to guide the modeling at the level of sensitivity targeted by future CMB spectroscopy.

Additional important foreground components are due to anomalous microwave emission (Draine & Lazarian 1998; Ali-Haïmoud et al. 2009; Planck Collaboration et al. 2011), various narrow molecular lines (e.g., CO, HCN, HCO, etc.), zodiacal light (Planck Collaboration et al. 2014b) and the integrated flux of CO emission throughout cosmic history (Righi et al. 2008; Mashian et al. 2016), all of which will also affect future CMB imaging experiments. In all cases, one will have to make use of properties of the underlying physical mechanism to motivate refined foreground parametrizations. The primordial distortion signals caused by energy release are all *unpolarized*, which is another important property to exploit. Systematic effects related to the absolute calibration could furthermore be tested using the motion-induced leakage of monopole signals into the CMB dipole (Balashev et al. 2015). It was also pointed out that the relativistic correction signal (see Sect. 2.1) could cause significant confusion for the r -distortion signals (Hill et al. 2015), which has to be modeled more carefully. All the above challenges need to be addressed to demonstrate the full potential and feasibility of future spectroscopic CMB experiments, a problem we are currently investigating. For additional recent discussion of the foreground separation problem for the CMB monopole see Sathyanarayana Rao et al. (2015), Desjacques et al. (2015) and De Zotti et al. (2015).

5 CONCLUSIONS

Within Λ CDM, a range of guaranteed distortion signals is expected. Here, we summarized these distortions and also provided an assessment of the expected uncertainties in their prediction (Sect. 2 and Fig. 1). The largest signals is due to the formation of structures and reionization process at late times (Sect. 2.1). The signal

is characterized by a y -type spectrum, with a y -parameter reaching $\approx \text{few} \times 10^{-6}$. Although the uncertainty in the amplitude of this contribution is rather large, this signal will be detectable with a *PIXIE*-like experiment at very high significance, even allowing us to determine the small relativistic temperature correction caused by abundant low-mass haloes with temperature $T_e \approx 10^6$ K (see Hill et al. 2015). This promises a way to solve the missing baryon problem and constrain the first sources of reionization.

The largest primordial signal expected within Λ CDM is due to the damping of small-scale acoustic modes (Sect. 2.2). The y -distortion contribution is swamped by the low-redshift signal, but the μ -distortion should be detectable with a slightly improved version of *PIXIE*. Using *Planck* data, we find $\mu \approx (2.00 \pm 0.14) \times 10^{-8}$ for the standard Λ CDM cosmology, where the uncertainty is dominated by those of power spectrum parameters. This value includes the fact that temperature shift, μ , y and r -distortions are not uniquely separable, but that these parameters have to be determined simultaneously. As our comparison of different approximation methods shows (Sect. 3.1), simple estimates for μ , based solely on scattering physics arguments, are expected to underestimate the recovered/measured value obtained with future distortion experiments by $\approx 20\% - 30\%$ (see Table 1).

Our simple forecasts show (Sect. 4), that by combining CMB spectral distortion measurements with existing *Planck* data, one can achieve an $\approx 40\% - 50\%$ improvement of the error on n_{run} for ≈ 3.4 times the sensitivity of *PIXIE*. At this sensitivity, also an $\approx 5\sigma$ detection of μ from distortion measurements alone can be expected. About ≈ 10 times the sensitivity of *PIXIE* is required for a marginal $\approx 2.6\sigma$ detection of the first r -distortion parameter, $\mu_1 \approx (3.82 \pm 0.22) \times 10^{-8}$, assuming Λ CDM. This sensitivity would furthermore render the CRR detectable at the level of a few σ (Desjacques et al. 2015) and deliver a factor of ≈ 3 improvement of the error on n_{run} (Fig. 5 and Table 3). A combination of CMB spectral distortion measurements with upcoming ground-based experiments (e.g., Stage-IV CMB) could help further tightening constraints on power spectrum parameters and neutrino physics; however, enhanced versions of *PIXIE* are required to achieve this.

In Sect. 4.1, we gave a brief discussion of the spectral distortion foreground challenge. Simple, physically-motivated extensions of the foreground parametrizations are required to capture the effect of averaging of spatially varying spectral components inside the instrumental beam and across the sky. While existing data can be used to inform the underlying models, at the high sensitivity targeted by future spectroscopic missions, these foreground parameters ultimately have to be determined in the measurements. FTS concepts provide many hundred channels, which should allow us to extend the parameter list of refined foreground models from a few to tens, promising a path towards detailed spectral distortion measurements that we will investigate in the future.

We close by mentioning that in spite of all the successes of Λ CDM, there are open puzzles, such as the nature of dark matter and dark energy, to name the obvious ones. Spectral distortions are sensitive to *new physics* and any departure from the expected Λ CDM predictions for the high- z signals will inevitably point in this direction. For example, if at early times dark matter coupled to baryons or photons, then this will leave an effect on the CMB spectrum (e.g., Ali-Haïmoud et al. 2015), potentially diminishing the net distortion. Also, significantly higher or significantly lower power at small scales, responsible for the μ -distortion signal ($k \approx 740 \text{ Mpc}^{-1}$), are necessarily related to departures from simple slow-roll inflation (Chluba et al. 2012a; Chluba & Jeong 2014; Clesse et al. 2014; Chluba et al. 2015b; Cabass et al. 2016). The

presence of unaccounted relicts (e.g., gravitinos or moduli) or excited states of dark matter, decaying early enough to leave the CMB anisotropies unaffected, could furthermore play a role (Hu & Silk 1993b; Chluba & Sunyaev 2012; Chluba 2013a; Chluba & Jeong 2014; Dimastrogiovanni et al. 2015).

This illustrates only a few of the interesting new directions that CMB spectral distortions measurements could shed light on, and the big challenge will be to disentangle different effects to allow us draw clear conclusions. We can only look forward to the advent of real distortion data in the future.

ACKNOWLEDGEMENTS

JC cordially thanks Nick Battaglia, Giovanni Cabass, Colin Hill, Alessandro Melchiorri and Enrico Pajer for valuable feedback on the manuscript, and Steven Gratton for helpful advice on *Planck* data. JC is supported by the Royal Society as a Royal Society University Research Fellow at the University of Manchester, UK.

REFERENCES

- Abazajian K. N. et al., 2015a, *Astroparticle Physics*, 63, 55
 Abazajian K. N. et al., 2015b, *Astroparticle Physics*, 63, 66
 Adriani O. et al., 2009, *Nature*, 458, 607
 Ali-Haïmoud Y., 2013, *Phys.Rev.D*, 87, 023526
 Ali-Haïmoud Y., Chluba J., Kamionkowski M., 2015, *Physical Review Letters*, 115, 071304
 Ali-Haïmoud Y., Hirata C. M., 2011, *Phys.Rev.D*, 83, 043513
 Ali-Haïmoud Y., Hirata C. M., Dickinson C., 2009, *MNRAS*, 395, 1055
 André P. et al., 2014, *JCAP*, 2, 6
 Aslanyan G., Price L. C., Adams J., Bringmann T., Clark H. A., Easther R., Lewis G. F., Scott P., 2015, *ArXiv:1512.04597*
 Balashev S. A., Kholupenko E. E., Chluba J., Ivanchik A. V., Varshalovich D. A., 2015, *ApJ*, 810, 131
 Barrow J. D., Coles P., 1991, *MNRAS*, 248, 52
 Basu K., Hernández-Monteagudo C., Sunyaev R. A., 2004, *A&A*, 416, 447
 Battaglia N., Bond J. R., Pfrommer C., Sievers J. L., Sijacki D., 2010, *ApJ*, 725, 91
 Baumann D., 2009, *ArXiv:0907.5424*
 Bennett C. L. et al., 2003, *ApJS*, 148, 1
 Bertone G., Hooper D., Silk J., 2005, *Physics Reports*, 405, 279
 Biagetti M., Perrier H., Riotto A., Desjacques V., 2013, *Phys.Rev.D*, 87, 063521
 Birkinshaw M., 1999, *Physics Reports*, 310, 97
 Bringmann T., Scott P., Akrami Y., 2012, *Phys.Rev.D*, 85, 125027
 Burigana C., Danese L., de Zotti G., 1991, *A&A*, 246, 49
 Cabass G., Melchiorri A., Pajer E., 2016, *ArXiv:1602.05578*
 Carlstrom J. E., Holder G. P., Reese E. D., 2002, *ARA&A*, 40, 643
 CDMS II Collaboration et al., 2010, *Science*, 327, 1619
 Cen R., Ostriker J. P., 1999, *ApJ*, 514, 1
 Chen X., Kamionkowski M., 2004, *Phys.Rev.D*, 70, 043502
 Chluba J., 2005, PhD thesis, LMU München
 Chluba J., 2010, *MNRAS*, 402, 1195
 Chluba J., 2011, *MNRAS*, 415, 3227
 Chluba J., 2013a, *MNRAS*, 436, 2232
 Chluba J., 2013b, *MNRAS*, 434, 352
 Chluba J., 2014, *MNRAS*, 440, 2544
 Chluba J., 2015, *ArXiv:1506.06582*
 Chluba J., Ali-Haïmoud Y., 2016, *MNRAS*, 456, 3494
 Chluba J., Dai L., Grin D., Amin M. A., Kamionkowski M., 2015a, *MNRAS*, 446, 2871
 Chluba J., Erickcek A. L., Ben-Dayana I., 2012a, *ApJ*, 758, 76
 Chluba J., Grin D., 2013, *MNRAS*, 434, 1619
 Chluba J., Hamann J., Patil S. P., 2015b, *International Journal of Modern Physics D*, 24, 1530023
 Chluba J., Jeong D., 2014, *MNRAS*, 438, 2065
 Chluba J., Khatri R., Sunyaev R. A., 2012b, *MNRAS*, 425, 1129
 Chluba J., Nagai D., Sazonov S., Nelson K., 2012c, *MNRAS*, 426, 510
 Chluba J., Rubiño-Martín J. A., Sunyaev R. A., 2007, *MNRAS*, 374, 1310
 Chluba J., Sunyaev R. A., 2004, *A&A*, 424, 389
 Chluba J., Sunyaev R. A., 2006, *A&A*, 458, L29
 Chluba J., Sunyaev R. A., 2008, *A&A*, 478, L27
 Chluba J., Sunyaev R. A., 2009, *A&A*, 501, 29
 Chluba J., Sunyaev R. A., 2010, *MNRAS*, 402, 1221
 Chluba J., Sunyaev R. A., 2012, *MNRAS*, 419, 1294
 Chluba J., Switzer E., Nelson K., Nagai D., 2013, *MNRAS*, 430, 3054
 Chluba J., Thomas R. M., 2011, *MNRAS*, 412, 748
 Chluba J., Vasil G. M., Dursi L. J., 2010, *MNRAS*, 407, 599
 Cirelli M., Iocco F., Panci P., 2009, *JCAP*, 10, 9
 Clesse S., Garbrecht B., Zhu Y., 2014, *ArXiv:1402.2257*
 Daly R. A., 1991, *ApJ*, 371, 14
 Danese L., de Zotti G., 1981, *A&A*, 94, L33
 Danese L., de Zotti G., 1982, *A&A*, 107, 39
 De Zotti G., Negrello M., Castex G., Lapi A., Bonato M., 2015, *ArXiv:1512.04816*
 Dent J. B., Easson D. A., Tashiro H., 2012, *Phys.Rev.D*, 86, 023514
 Desjacques V., Chluba J., Silk J., de Bernardis F., Doré O., 2015, *MNRAS*, 451, 4460
 Diamanti R., Lopez-Honorez L., Mena O., Palomares-Ruiz S., Vincent A. C., 2014, *JCAP*, 2, 017
 Diego J. M., Majumdar S., 2004, *MNRAS*, 352, 993
 Dimastrogiovanni E., Krauss L. M., Chluba J., 2015, *ArXiv:1512.09212*
 Dolag K., Komatsu E., Sunyaev R., 2015, *ArXiv:1509.05134*
 Draine B. T., Lazarian A., 1998, *ApJL*, 494, L19
 Dubrovich V. K., 1975, *Soviet Astronomy Letters*, 1, 196
 Dubrovich V. K., Stolyarov V. A., 1995, *A&A*, 302, 635
 Dubrovich V. K., Stolyarov V. A., 1997, *Astronomy Letters*, 23, 565
 Emami R., Dimastrogiovanni E., Chluba J., Kamionkowski M., 2015, *Phys.Rev.D*, 91, 123531
 Finkbeiner D. P., Davis M., Schlegel D. J., 1999, *ApJ*, 524, 867
 Fixsen D. J., 2009, *ApJ*, 707, 916
 Fixsen D. J., Cheng E. S., Gales J. M., Mather J. C., Shafer R. A., Wright E. L., 1996, *ApJ*, 473, 576
 Galli S., Iocco F., Bertone G., Melchiorri A., 2009, *Phys.Rev.D*, 80, 023505
 Galli S., Slatyer T. R., Valdes M., Iocco F., 2013, *Phys.Rev.D*, 88, 063502
 Ganc J., Komatsu E., 2012, *Phys.Rev.D*, 86, 023518
 Giesen G., Lesgourgues J., Audren B., Ali-Haïmoud Y., 2012, *JCAP*, 12, 8
 Hernández-Monteagudo C., Rubiño-Martín J. A., Sunyaev R. A., 2007, *MNRAS*, 380, 1656
 Hill J. C., Battaglia N., Chluba J., Ferraro S., Schaan E., Spergel D. N., 2015, *Physical Review Letters*, 115, 261301
 Hinshaw G. et al., 2009, *ApJS*, 180, 225
 Hu W., 1995, *arXiv:astro-ph/9508126*
 Hu W., Scott D., Silk J., 1994a, *ApJL*, 430, L5
 Hu W., Scott D., Silk J., 1994b, *Phys.Rev.D*, 49, 648
 Hu W., Silk J., 1993a, *Phys.Rev.D*, 48, 485
 Hu W., Silk J., 1993b, *Physical Review Letters*, 70, 2661
 Hu W., Sugiyama N., 1994, *ApJ*, 436, 456
 Hütsi G., Chluba J., Hektor A., Raidal M., 2011, *A&A*, 535, A26
 Hütsi G., Hektor A., Raidal M., 2009, *A&A*, 505, 999
 Inogamov N. A., Sunyaev R. A., 2015, *Astronomy Letters*, 41, 693
 Irfan M. O. et al., 2015, *MNRAS*, 448, 3572
 Jungman G., Kamionkowski M., Griest K., 1996, *Physics Reports*, 267, 195
 Kaiser N., 1983, *MNRAS*, 202, 1169
 Kamionkowski M., Knox L., 2003, *Phys.Rev.D*, 67, 063001
 Khatri R., Sunyaev R. A., 2012a, *JCAP*, 9, 16
 Khatri R., Sunyaev R. A., 2012b, *JCAP*, 6, 38
 Khatri R., Sunyaev R. A., 2013, *JCAP*, 6, 26

- Khatri R., Sunyaev R. A., Chluba J., 2012, *A&A*, 540, A124
- Kholupenko E. E., Ivanchik A. V., Varshalovich D. A., 2005, *Gravitation and Cosmology*, 11, 161
- Kogut A. et al., 2011, *JCAP*, 7, 25
- Komatsu E., Seljak U., 2002, *MNRAS*, 336, 1256
- Lewis A., 2013, *JCAP*, 8, 053
- Loeb A., 2001, *ApJL*, 555, L1
- Mashian N., Loeb A., Sternberg A., 2016, *MNRAS*
- McDonald P., Scherrer R. J., Walker T. P., 2001, *Phys.Rev.D*, 63, 023001
- Miniati F., Ryu D., Kang H., Jones T. W., Cen R., Ostriker J. P., 2000, *ApJ*, 542, 608
- Munshi D., Joudaki S., Smidt J., Coles P., Kay S. T., 2013, *MNRAS*, 429, 1564
- Oh S. P., Cooray A., Kamionkowski M., 2003, *MNRAS*, 342, L20
- Ota A., Takahashi T., Tashiro H., Yamaguchi M., 2014, *JCAP*, 10, 29
- Padmanabhan N., Finkbeiner D. P., 2005, *Phys.Rev.D*, 72, 023508
- Page L. et al., 2007, *ApJS*, 170, 335
- Pajer E., Zaldarriaga M., 2012, *Physical Review Letters*, 109, 021302
- Pajer E., Zaldarriaga M., 2013, *JCAP*, 2, 36
- Peebles P. J. E., 1968, *ApJ*, 153, 1
- Pitrou C., Bernardeau F., Uzan J.-P., 2010, *JCAP*, 7, 19
- Planck Collaboration et al., 2015a, *ArXiv:1502.01588*
- Planck Collaboration et al., 2014a, *A&A*, 571, A12
- Planck Collaboration et al., 2014b, *A&A*, 571, A14
- Planck Collaboration et al., 2014c, *A&A*, 571, A15
- Planck Collaboration et al., 2014d, *A&A*, 571, A16
- Planck Collaboration et al., 2014e, *A&A*, 571, A21
- Planck Collaboration et al., 2011, *A&A*, 536, A20
- Planck Collaboration et al., 2015b, *ArXiv:1502.01589*
- Planck Collaboration et al., 2015c, *ArXiv:1507.02704*
- Planck Collaboration et al., 2015d, *ArXiv:1502.01596*
- Refregier A., Komatsu E., Spergel D. N., Pen U.-L., 2000, *Phys.Rev.D*, 61, 123001
- Remazeilles M., Dickinson C., Eriksen H. K. K., Wehus I. K., 2015, *ArXiv:1509.04714*
- Righi M., Hernández-Monteagudo C., Sunyaev R. A., 2008, *A&A*, 489, 489
- Rubiño-Martín J. A., Chluba J., Sunyaev R. A., 2006, *MNRAS*, 371, 1939
- Rubiño-Martín J. A., Chluba J., Sunyaev R. A., 2008, *A&A*, 485, 377
- Rubiño-Martín J. A., Hernández-Monteagudo C., Sunyaev R. A., 2005, *A&A*, 438, 461
- Rybicki G. B., dell’Antonio I. P., 1993, in *ASP Conf. Ser. 51: Observational Cosmology*, Chincarini G. L., Iovino A., Maccacaro T., Maccagni D., eds., pp. 548–
- Sathyanarayana Rao M., Subrahmanyam R., Udaya Shankar N., Chluba J., 2015, *ApJ*, 810, 3
- Shaw L. D., Nagai D., Bhattacharya S., Lau E. T., 2010, *ApJ*, 725, 1452
- Shull J. M., van Steenberg M. E., 1985, *ApJ*, 298, 268
- Slatyer T. R., 2016, *Phys.Rev.D*, 93, 023521
- Slatyer T. R., Padmanabhan N., Finkbeiner D. P., 2009, *Physical Review D (Particles, Fields, Gravitation, and Cosmology)*, 80, 043526
- Smirnov A. V. et al., 2012, in *SPIE Conference Series*, Vol. 8442
- Starobinsky A. A., 1980, *Physics Letters B*, 91, 99
- Stebbins A., 2007, *astro-ph/0703541*
- Steigman G., 2007, *Annual Review of Nuclear and Particle Science*, 57, 463
- Sunyaev R. A., Chluba J., 2009, *Astronomische Nachrichten*, 330, 657
- Sunyaev R. A., Khatri R., 2013, *International Journal of Modern Physics D*, 22, 30014
- Sunyaev R. A., Zeldovich I. B., 1980, *MNRAS*, 190, 413
- Sunyaev R. A., Zeldovich Y. B., 1970a, *ApSS*, 9, 368
- Sunyaev R. A., Zeldovich Y. B., 1970b, *ApSS*, 7, 20
- Sunyaev R. A., Zeldovich Y. B., 1972, *A&A*, 20, 189
- Tashiro H., 2014, *Prog. of Theo. and Exp. Physics*, 2014, 060000
- Valdés M., Evoli C., Ferrara A., 2010, *MNRAS*, 404, 1569
- Weinberg S., 1971, *ApJ*, 168, 175
- Yu Q., Spergel D. N., Ostriker J. P., 2001, *ApJ*, 558, 23
- Zaldarriaga M., Loeb A., 2002, *ApJ*, 564, 52
- Zavala J., Vogelsberger M., Slatyer T. R., Loeb A., Springel V., 2011, *Phys.Rev.D*, 83, 123513
- Zeldovich Y. B., Illarionov A. F., Sunyaev R. A., 1972, *SJETP*, 35, 643
- Zeldovich Y. B., Kurt V. G., Sunyaev R. A., 1968, *Zhurnal Eksperimentalnoi i Teoreticheskoi Fiziki*, 55, 278
- Zeldovich Y. B., Sunyaev R. A., 1969, *ApSS*, 4, 301
- Zhang L., Chen X., Lei Y., Si Z., 2006, *Phys.Rev.D*, 74, 103519
- Zhang P., Pen U.-L., Trac H., 2004, *MNRAS*, 355, 451